

Heavy-Section Steel Technology Program Quarterly Progress Report for January-March 1978

G. D. Whitman
R. H. Bryan

Prepared for the U.S. Nuclear Regulatory Commission
Office of Nuclear Regulatory Research
Under Interagency Agreements DOE 40-551-75 and 40-552-75

OAK RIDGE NATIONAL LABORATORY
OPERATED BY UNION CARBIDE CORPORATION • FOR THE DEPARTMENT OF ENERGY

7810136228

	<u>Page</u>
5.3.1 Fracture toughness investigations of the fabrication weld	27
5.3.2 Fractographic examination of ITV-8 fabrication weld	28
5.4 Investigation of Fracture Surfaces of ITV-6 Inside Surface Flaw	29
5.5 Crack-Arrest Tests	31
References	32
6. THERMAL SHOCK INVESTIGATIONS	33
6.1 Introduction	33
6.2 Cryogenic Quenching	33
6.3 PWR Double-Ended-Pipe-Break LOCA-ECC Parametric Analysis	38
References	45
7. FOREIGN RESEARCH	46
References	57

ORNL-DWG 78-5985

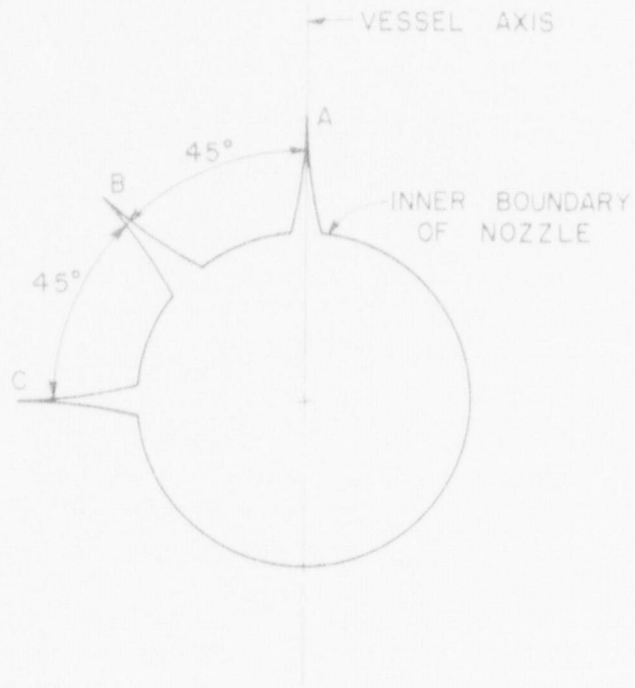


Fig. 2.1. Crack orientation relative to vessel axis (A, phases I and II; B and C, phase III).

ORNL-DWG 78-10607

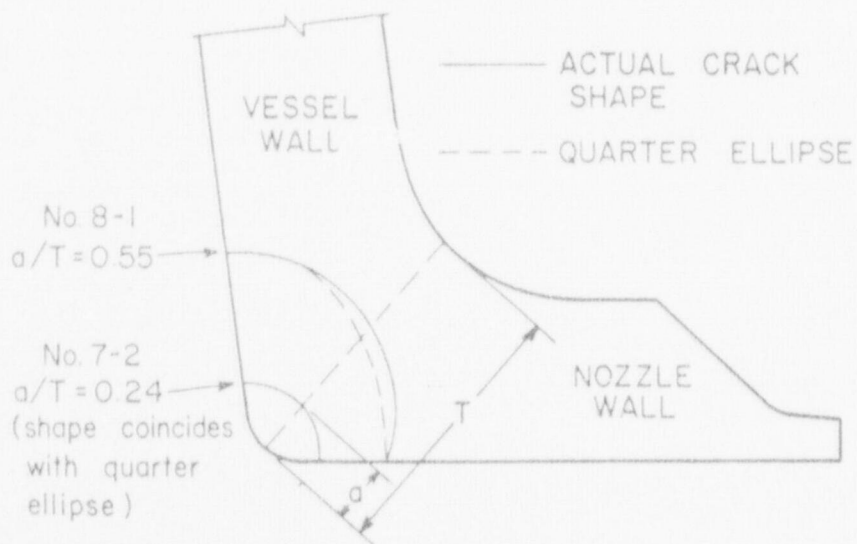


Fig. 2.2. Flaw shapes for type C cracks in a nozzle corner.

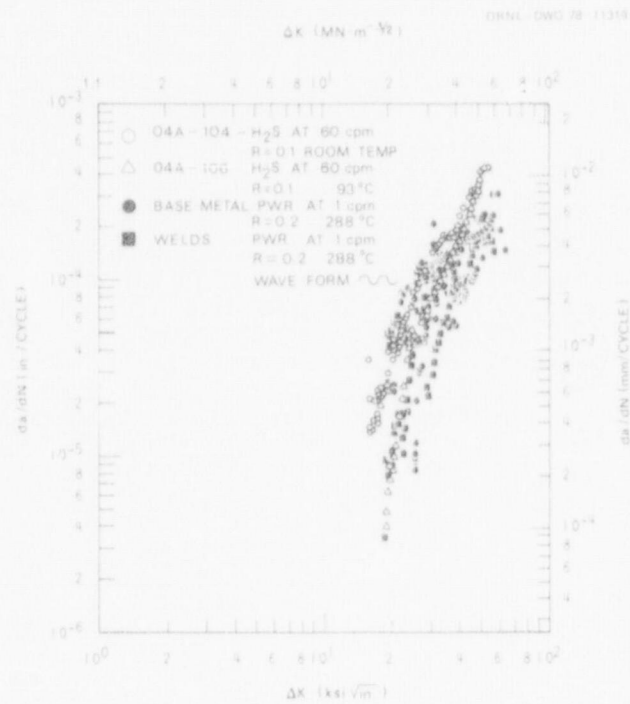


Fig. 3.1. Example of the effect of starting conditions on fatigue crack growth in pressure vessel steel in PWR environment (1T-CT data from Ref. 2).

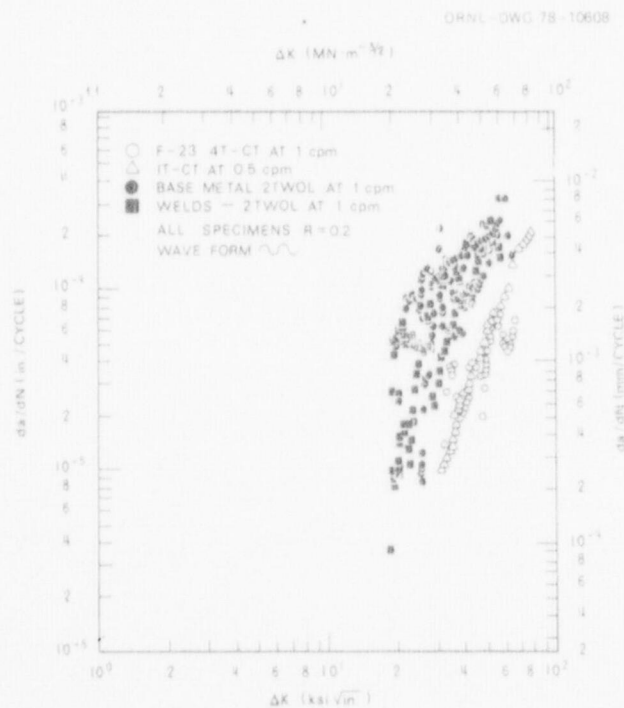


Fig. 3.2. Comparison of fatigue crack growth in pressure vessel steels in hydrogen sulfide and PWR environment - low R ratio.

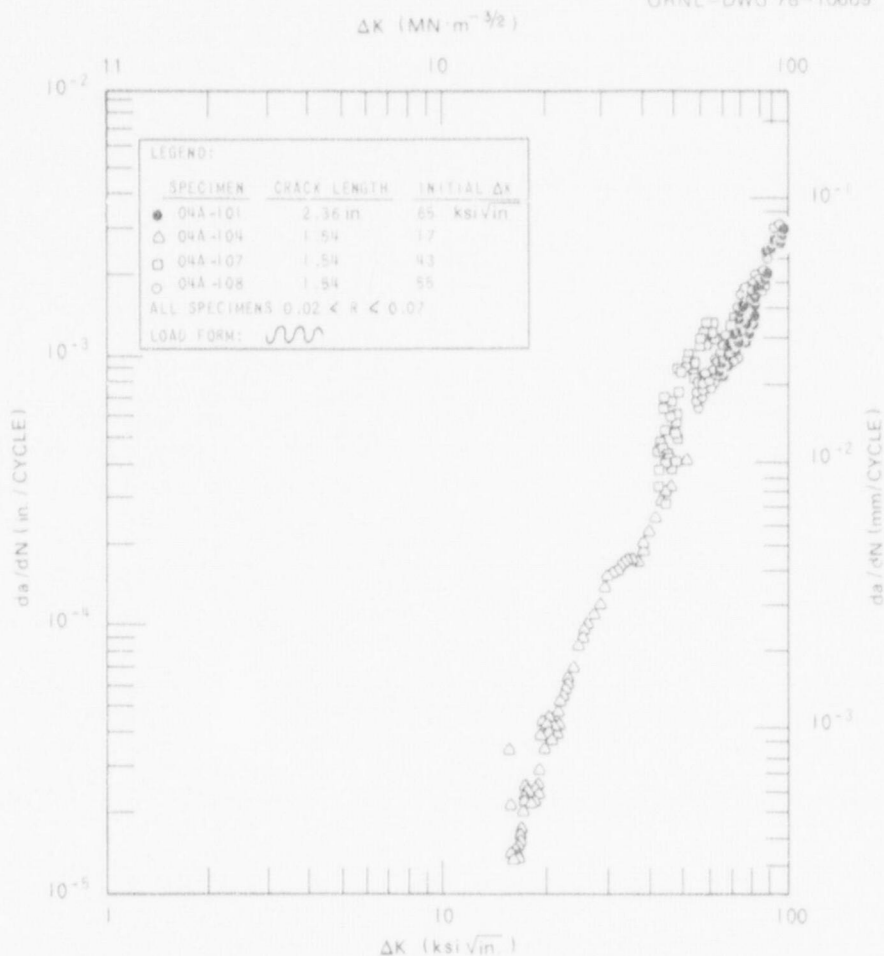


Fig. 3.3. Effect of starting conditions on fatigue-crack-growth rates in reactor pressure vessel steel in hydrogen sulfide at room temperature.

References

1. W. H. Bamford, D. M. Moon, and L. J. Ceschini, "Crack Growth Rate Testing in Reactor Pressure Vessel Steels," *Proceedings of Fifth Water Reactor Safety Information Meeting, Gaithersburg, Md.* (November 1977).
2. H. E. Watson, F. J. Loss, and B. H. Menke, "Fatigue Crack Propagation in LWR Materials," *Structural Integrity of Water Reactor Pressure Boundary Components - Progress Report Ending May 31, 1977*, Naval Research Laboratory, Washington, D.C.
3. P. M. Scott and D. R. V. Silvester, "The Influence of Mean Tensile Stress on Corrosion Fatigue Crack Growth in Structural Steel Immersed in Seawater," *United Kingdom Atomic Energy Authority Harwell Corrosion Service, Interim Technical Report UKOSRP 3/02* (May 1977).

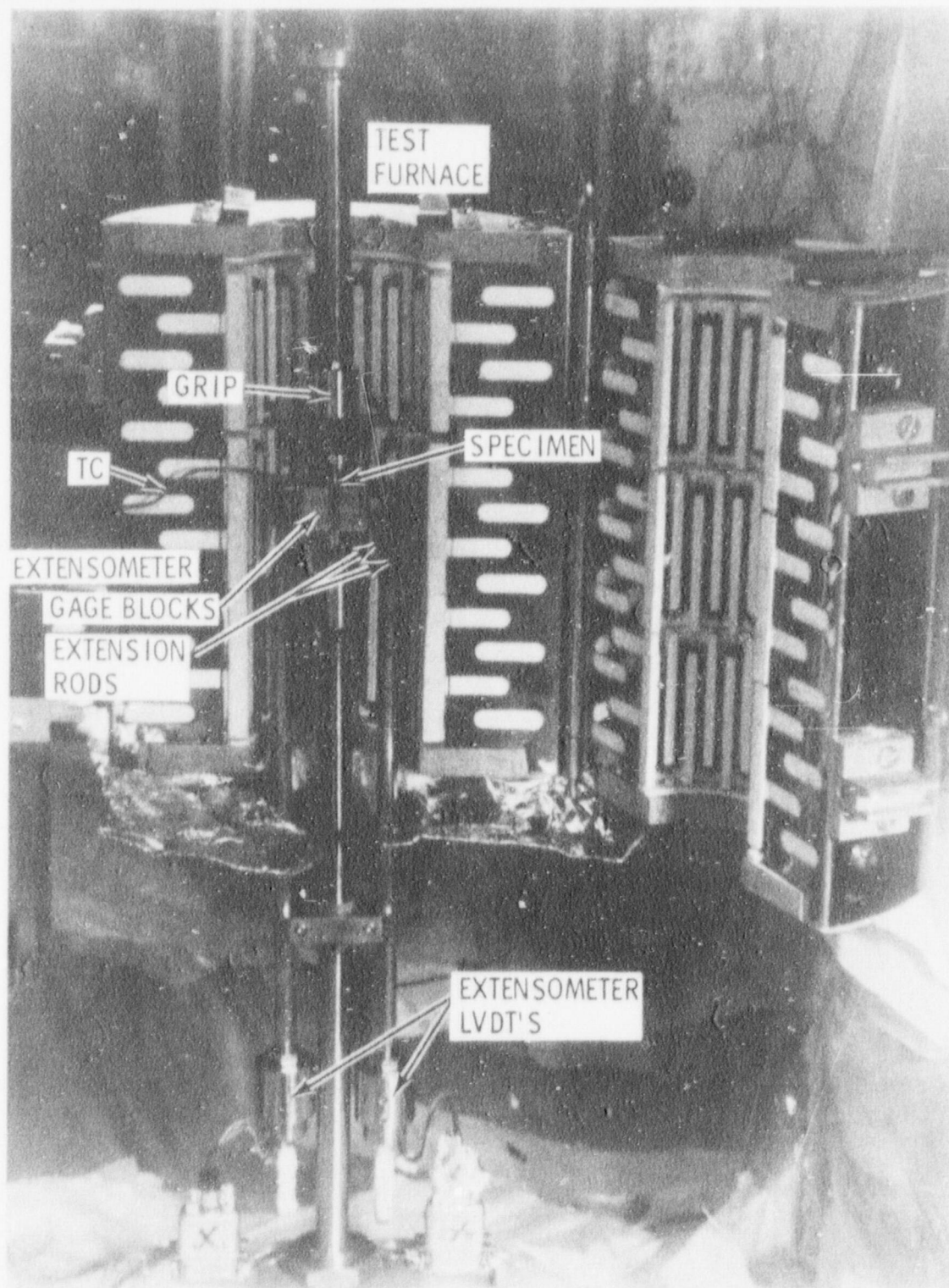


Fig. 4.1. Hot-cell test setup for irradiated tensile testing of specimens from 4T irradiations.



ORNL PHOTO 1635-78

Fig. 4.2. Fracture test data acquisition and processing system.

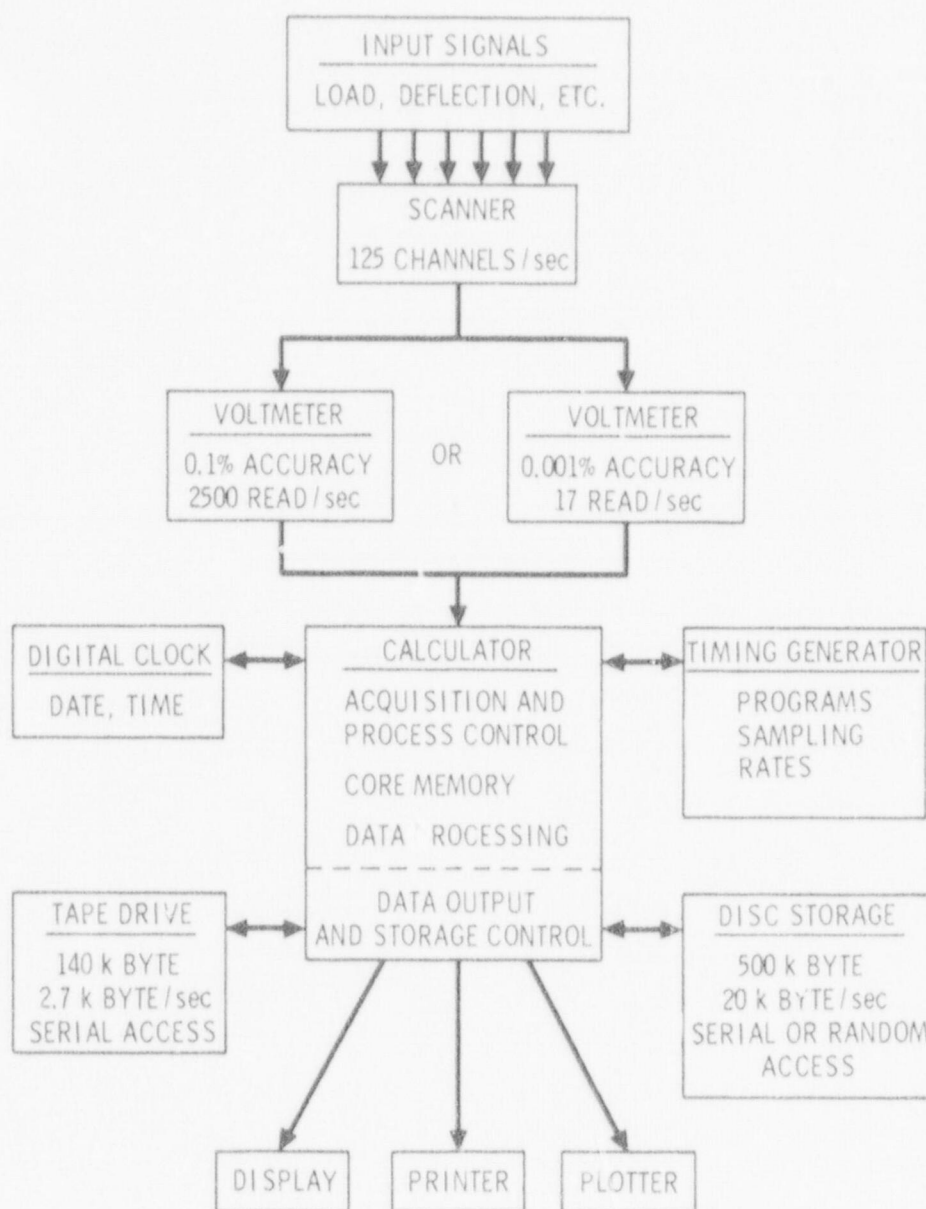


Fig. 4.3. Block diagram of data acquisition and processing system, showing general functions and capabilities.

blade reduces friction between the knife edge and the clip gage. Previously, knife edges on the load line of the specimen were machined into the specimen. In order to determine the difference between the razor blade knife edge and the machined-in knife edge, tests were conducted on both specimen types. The load vs load line displacement record for the razor blade knife edge is shown in Fig. 4.4. The relatively small amount of hysteresis and the parallel nature of both the loading and the unloading slopes should be noted. The load vs load line displacement curve for the specimen with a machined-in knife edge is shown in Fig. 4.5. The fact that the unloading curve has a distinctly different slope than the loading curve indicates a considerable amount of friction between the clip gage and the machined-in knife edge.

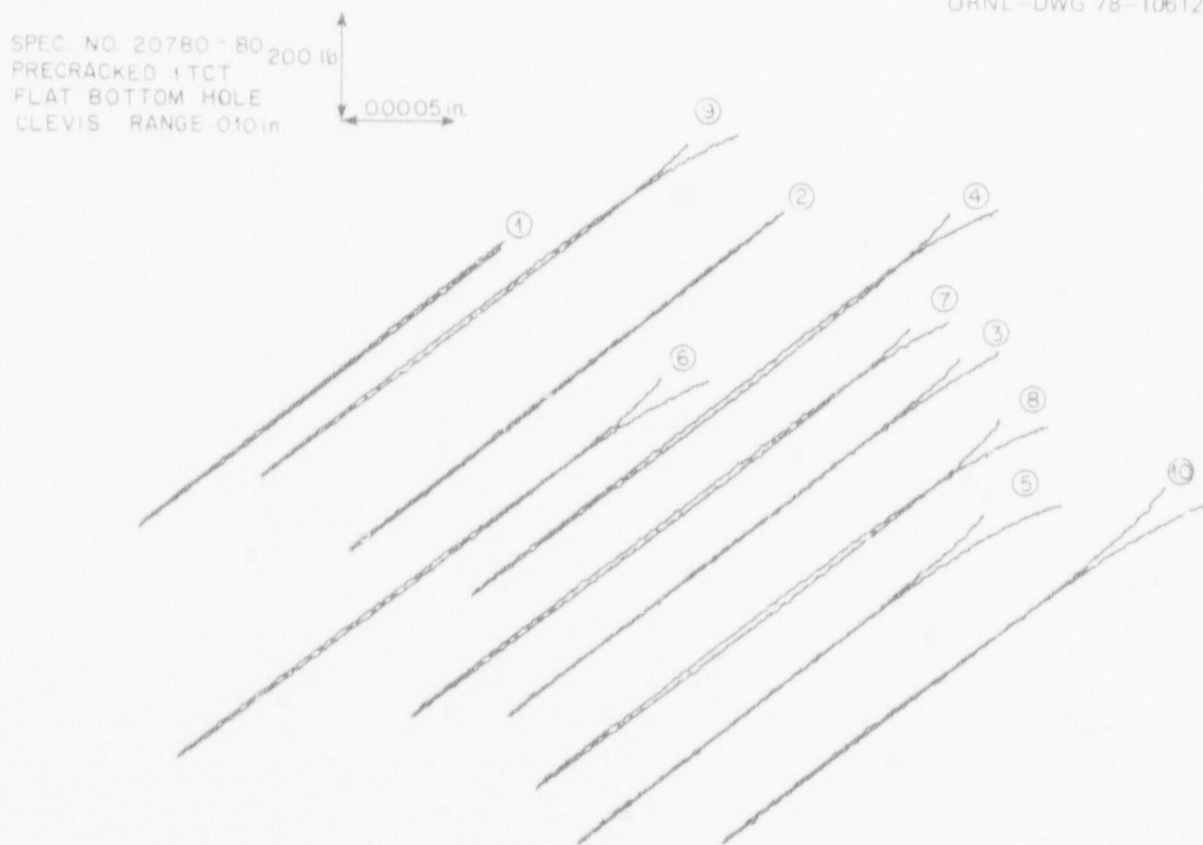


Fig. 4.4. Amplified load-displacement record for specimen with machined-in knife edge.

ORNL-DWG 78-10611

SPEC 20780-127
MACHINED KNIFE EDGE
0.100in RANGE USING
FLAT BOTTOM CLEVIS

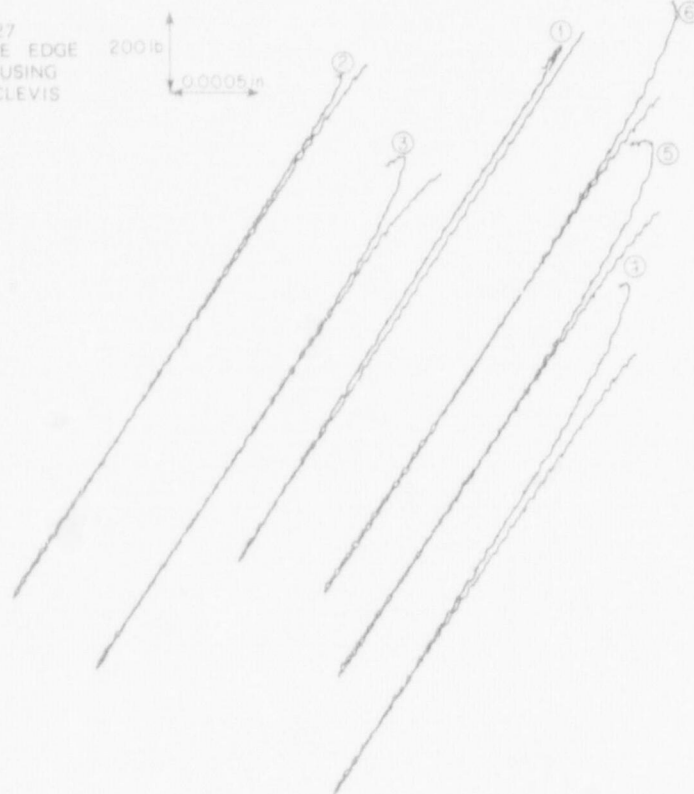


Fig. 4.5. Amplified load-displacement record for specimen with razor blade knife edge.

References

1. J. G. Merkle and H. T. Corten, "A J Integral Analysis for the Compact Specimen, Considering Axial Force as Well as Bending Effects," *Trans. ASME*, pp. 286-92, November 1974.
2. J. D. Landes, H. Walker, and G. A. Clarke, "Evaluation of Estimation Procedures Used in J Integral Testing," presented at the ASTM Symposium on Elastic Plastic Fracture Mechanics, Atlanta, Ga., November 1977.

5. PRESSURE VESSEL INVESTIGATIONS*

5.1 Posttest Examination of V-7B Flaw

P. P. Holz R. H. Bryan

The block of metal containing the flaw in intermediate test vessel V-7B was cut from the vessel for ultrasonic and destructive examination.¹ The block was examined by the Southwest Research Institute and the University of Michigan and returned to ORNL during the reporting period.

The block was saw cut transversely in 16 places as shown in Fig. 5.1. These cuts exposed cross-sectional views of the initial crack and the crack extension at 14 planes (28 faces). The etched faces of these cross sections show that the initial electron-beam weld crack lies entirely within the heat-affected zone (HAZ) of the weld repair as had been desired (see Fig. 5.2).

* Conversions from SI to English units for all SI quantities are listed on a foldout page at the end of this report.

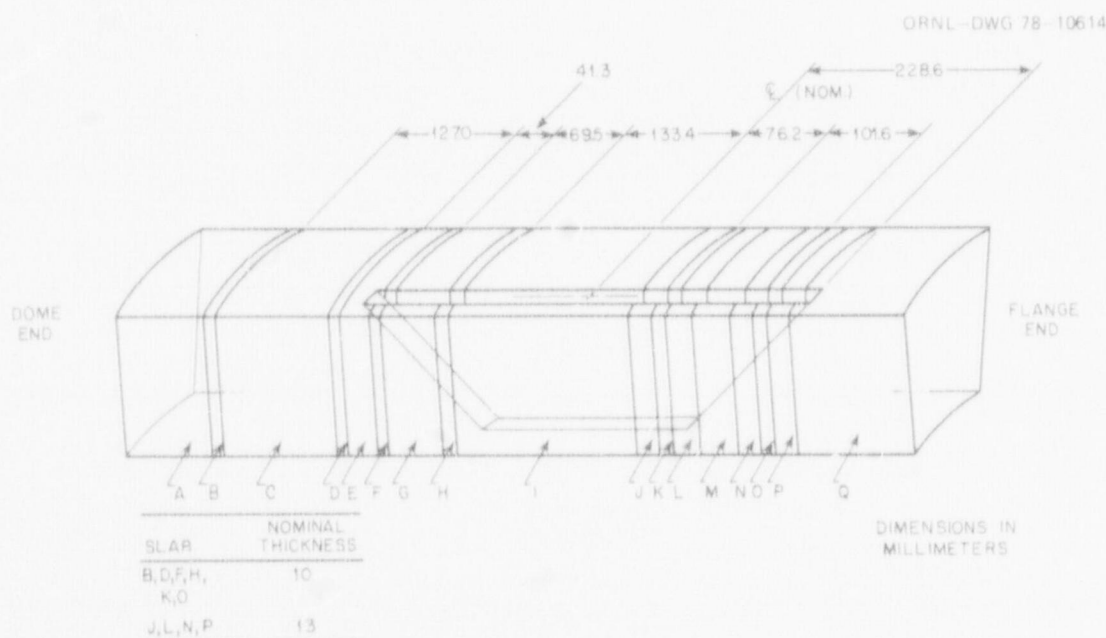


Fig. 5.1. Block cut from intermediate test vessel V-7B containing entire repair weld and fracture zone. Slabs A through Q were cut after all ultrasonic examinations were completed.

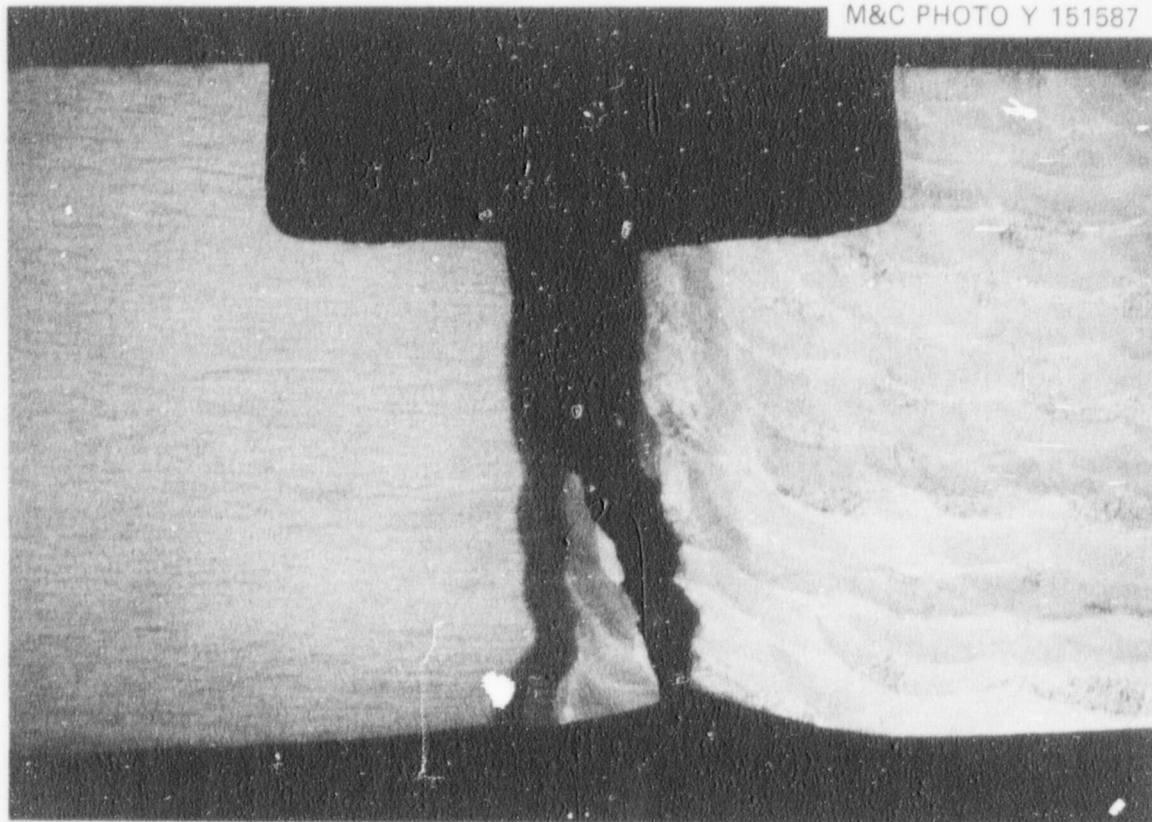


Fig. 5.2. Face K_f (the face of slab K nearest the flange end of the vessel) of cross section of V-7B fracture.

Segments J, K, and L (Fig. 5.1) fell in two pieces, since they were completely fractured during the test. Segments C, M, and Q were chilled in liquid nitrogen and broken open to expose the fracture surfaces. The two segments including the crack tips at both ends of the flaw (C and Q) are shown in Figs. 5.3 and 5.4, respectively. The visual examination of these pieces confirms the location of the crack front determined ultrasonically by K. K. Klindt.¹ It also appears that the crack extension lies entirely in the base metal in some regions, in weld metal in others, and in the HAZ only at crossover points. Figure 5.4 shows that the crack front curvature conforms to the interface of the weld and base metal. The location of the crack extension surfaces relative to the three types of metal (base, HAZ, and weld) will be determined by additional metallographic examination.

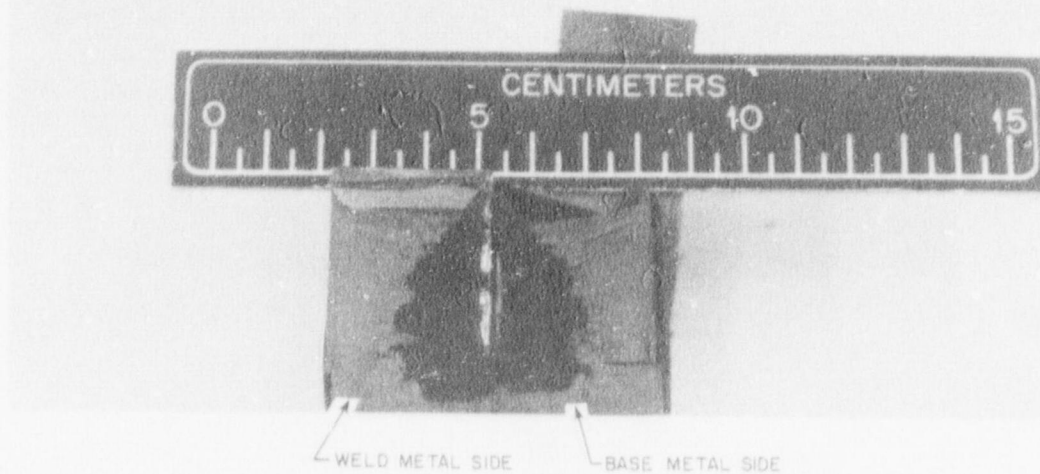


Fig. 5.3. V-7B fracture surfaces in slab C exposed by splitting the chilled slab.



Fig. 5.4. V-7B fracture surfaces in slab Q exposed by splitting the chilled slab.

5.2 Preparations for Intermediate Test Vessel V-8 Test

P. P. Holz

A 6.35-mm-wide longitudinal slot was machined into the center cylinder submerged-arc fabrication-seam weld of V-8, a distance of 19 mm from the approximately half-wall-thickness weld-repair edge, as shown in Fig. 5.5. A slitting saw cutter ground to a 30° included angle with a 0.127- to 0.191-mm tip radius was used for the final cuts to provide the tip of the notch with a sharp edge. A special stainless steel insert provided

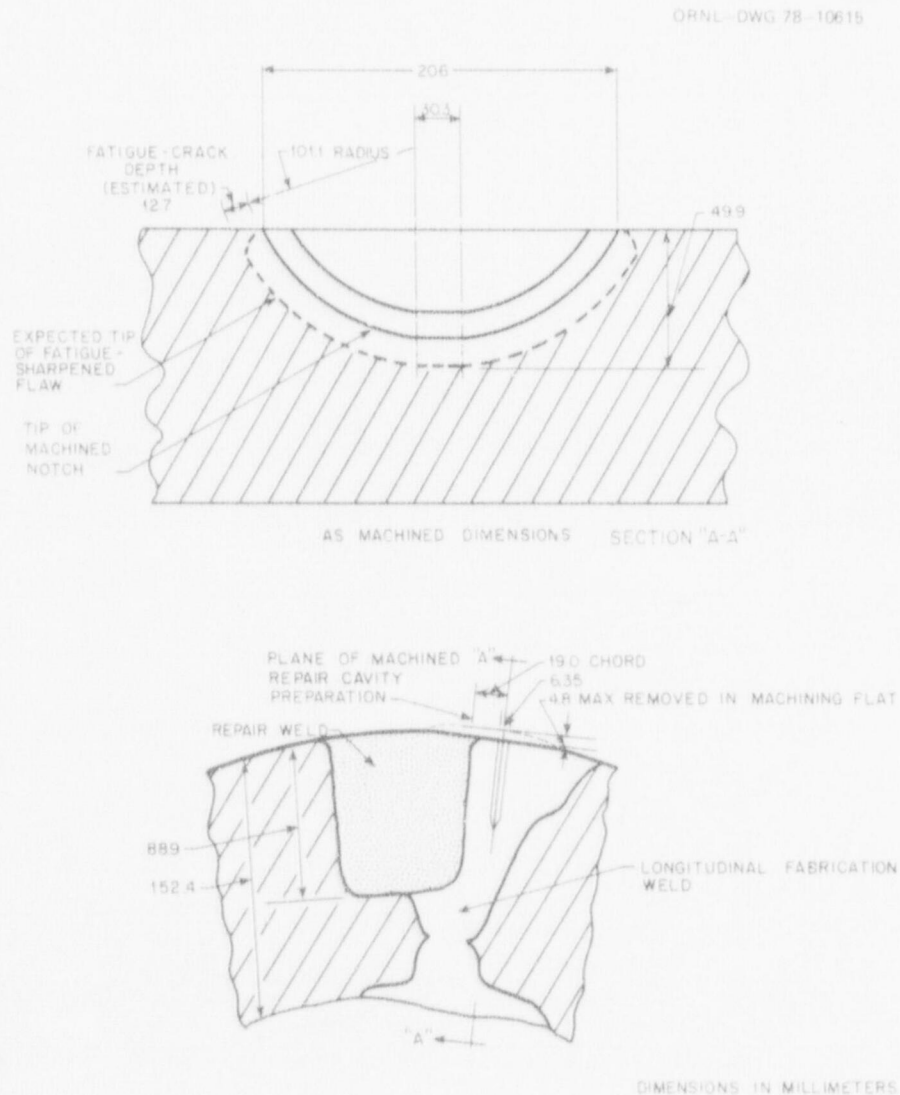


Fig. 5.5. Flaw details for intermediate test vessel V-8.

a tight-fitting plug for the slot and channeled the hydraulic pressurization fluid to the notch tip perimeter. Details of the machining and flaw pump setup duplicated the V-9 mockup previously used for prototype testing,² except that a large 152-mm Giddings and Lewis vertical boring mill was used for slotting the horizontally placed vessel as shown in Fig. 5.6.

Fifty strain gages were installed on the vessel in the region of the flaw to monitor changes in strain that occur as a result of residual stress relieved as the flaw is introduced. Tensile residual stresses were observed on the strain gages along the cut plane as the slitting saw first penetrated into the vessel wall. Later, during initial cyclic hydraulic pressurization of the notch to grow the flaw, strain readings taken in similar places implied that the original residual stress noted during slotting was considerable.

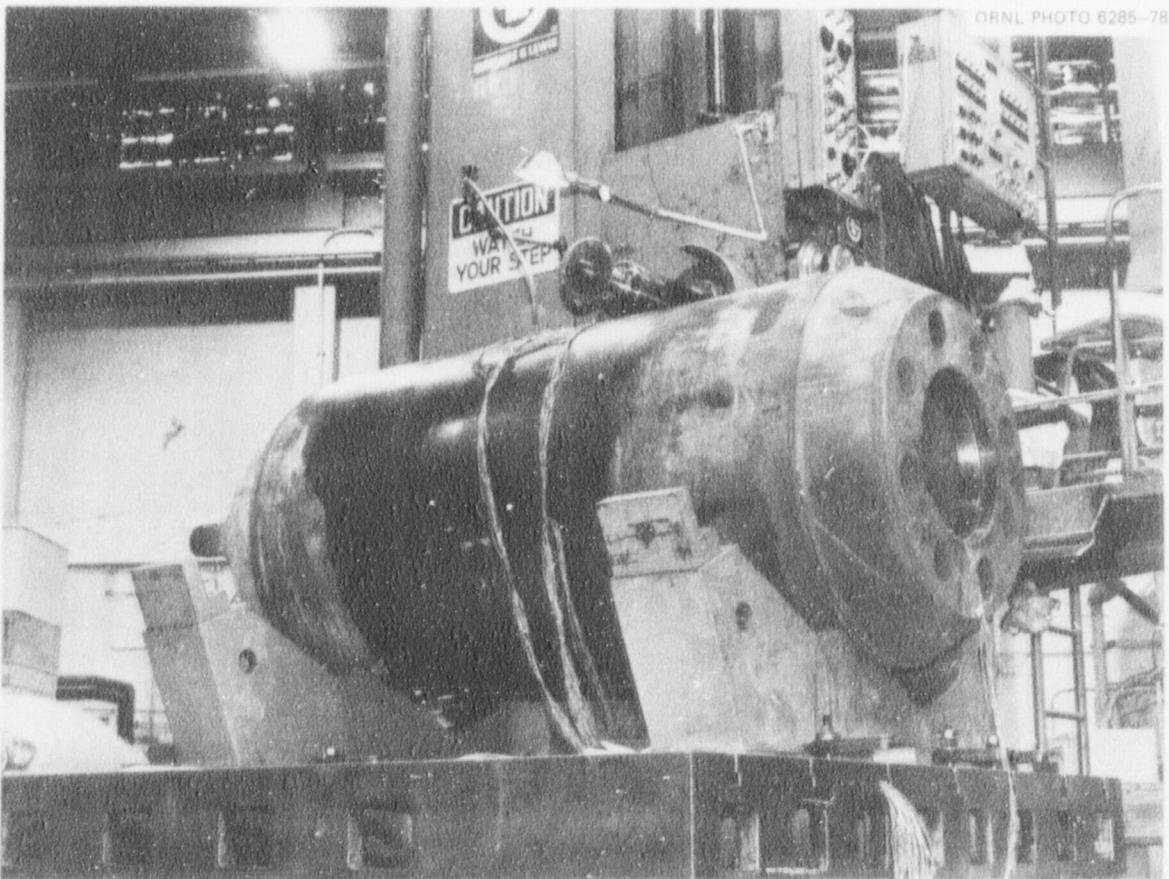


Fig. 5.6. Vertical boring mill slot machining for intermediate test vessel V-8.

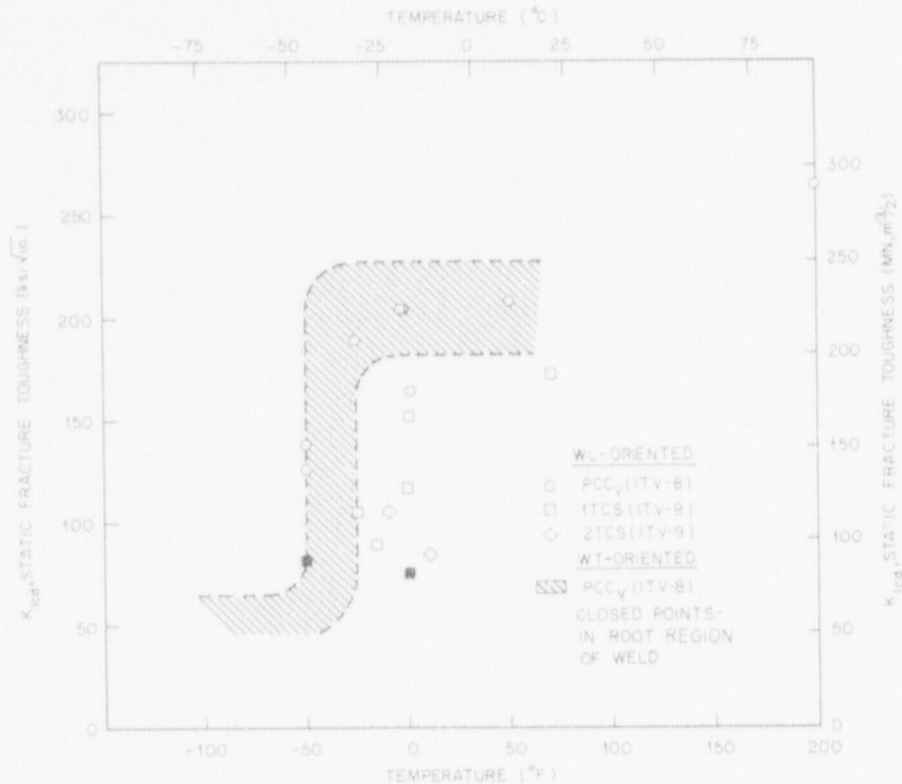


Fig. 5.7. Variation of static fracture toughness of the fabrication weld metal in the ITV-8 and ITV-9 prolongations from precracked Charpy and 1T and 2T compact specimens.

5.3.2 Fractographic examination of ITV-8 fabrication weld (D. A. Canonico and R. S. Crouse)

Previously,⁵ we reported a relationship between fracture toughness and the amount of dimple fracture at the fatigue crack tip in PCC_V specimens. Subsequently,⁴ a relationship was established among the microstructure at the PCC_V crack tip, the test temperature, and the fracture toughness. An example of this relationship is shown in Fig. 5.8. The narrow band of dimple fracture at the initiation site is 1×10^{-3} mm. The fracture toughness of this specimen (44 MPa√m at -46°C) was among the lowest obtained for the fabrication weld from the ITV-9 prolongation. Similar comparative studies are being conducted for PCC_V specimens that exhibited higher fracture toughness values at the -46°C test temperature.

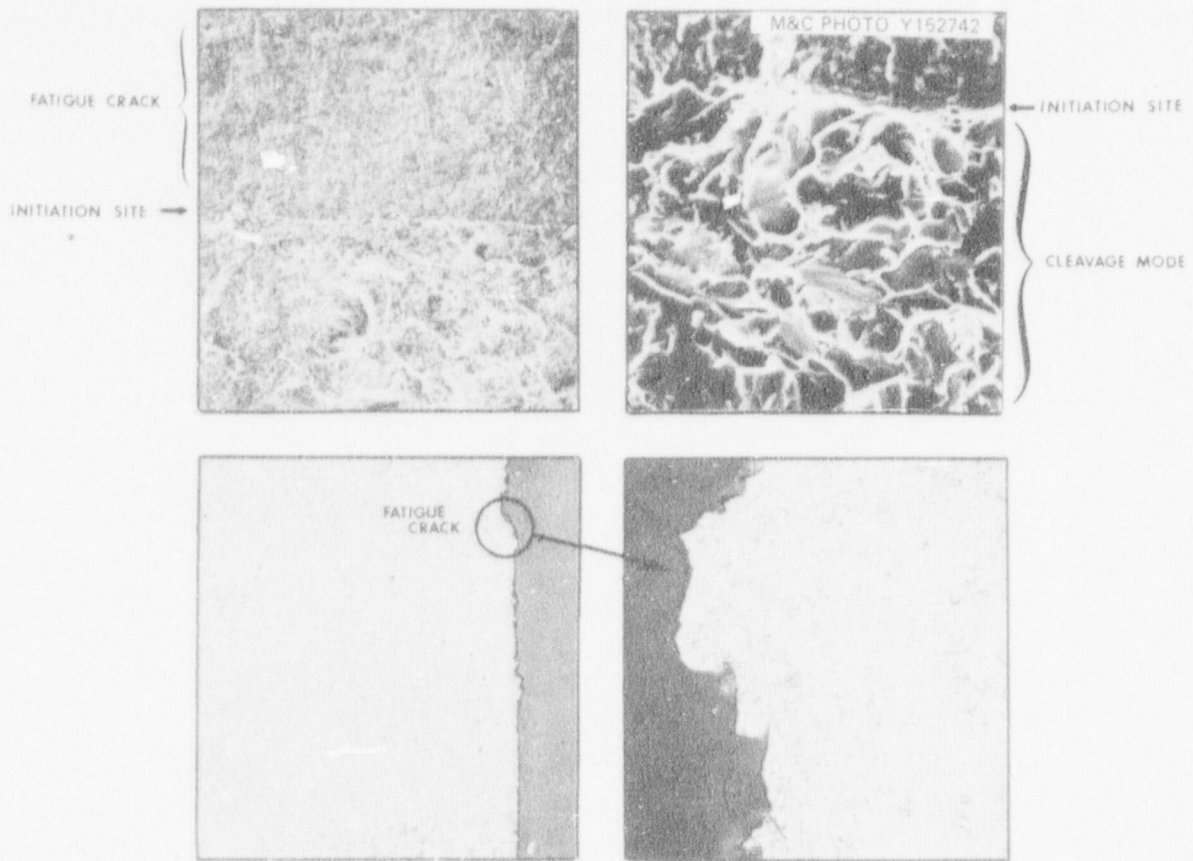


Fig. 5.8. Relationship between the microstructure at the fatigue crack tip in a precracked Charpy V-notch specimen; the amount of dimple fracture at the crack tip and the fracture toughness is illustrated. This specimen, V8W58, exhibited very poor toughness ($44 \text{ MPa} \sqrt{\text{m}}$) at -46°C . The width of the dimple region at the initiation site is very narrow ($1 \times 10^{-3} \text{ mm}$) and fracture is by cleavage mode. (Original reduced 31.5%)

5.4 Investigation of Fracture Surfaces of ITV-6 Inside Surface Flaw

P. P. Holz

A block was removed from ITV-6 containing flaw C, an inside surface flaw in the seam weld of the vessel cylinder.⁶ The block was chilled in liquid nitrogen and broken open along the plane of the crack to expose the fracture surfaces. The crack was examined to determine the amount of stable crack extension developed during the test of the vessel.

Figure 5.9 shows both crack faces; Fig. 5.10 shows one crack face and the profile of the crack at its deepest point obtained by cutting

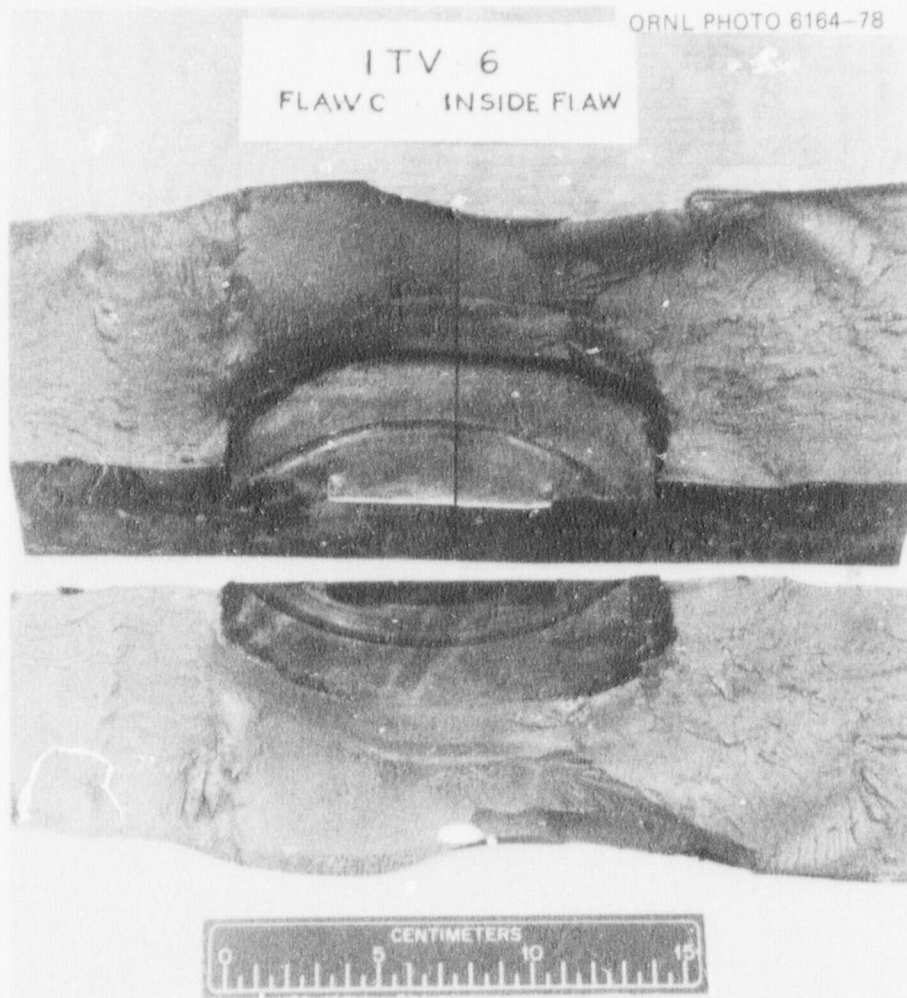


Fig. 5.9. Fracture surfaces of flaw C from intermediate test vessel V-6.

the other crack face piece in half. At the deepest point of the crack, the stable crack growth of the crack beyond the fatigue crack tip measures 6.4 mm. There is about the same amount of stable crack growth at other positions, but the plane of the stable crack growth changes from the fatigue crack plane at the deepest point to perpendicular to the crack plane at the surface. Vessel V-6 was the first intermediate test vessel to exhibit crack arrest. At a test temperature of 88°C the vessel failed at about 220 MPa. Final fracture was a full shear extending approximately 0.5 m from each end of flaw A, a similar flaw on the outside surface of the vessel.

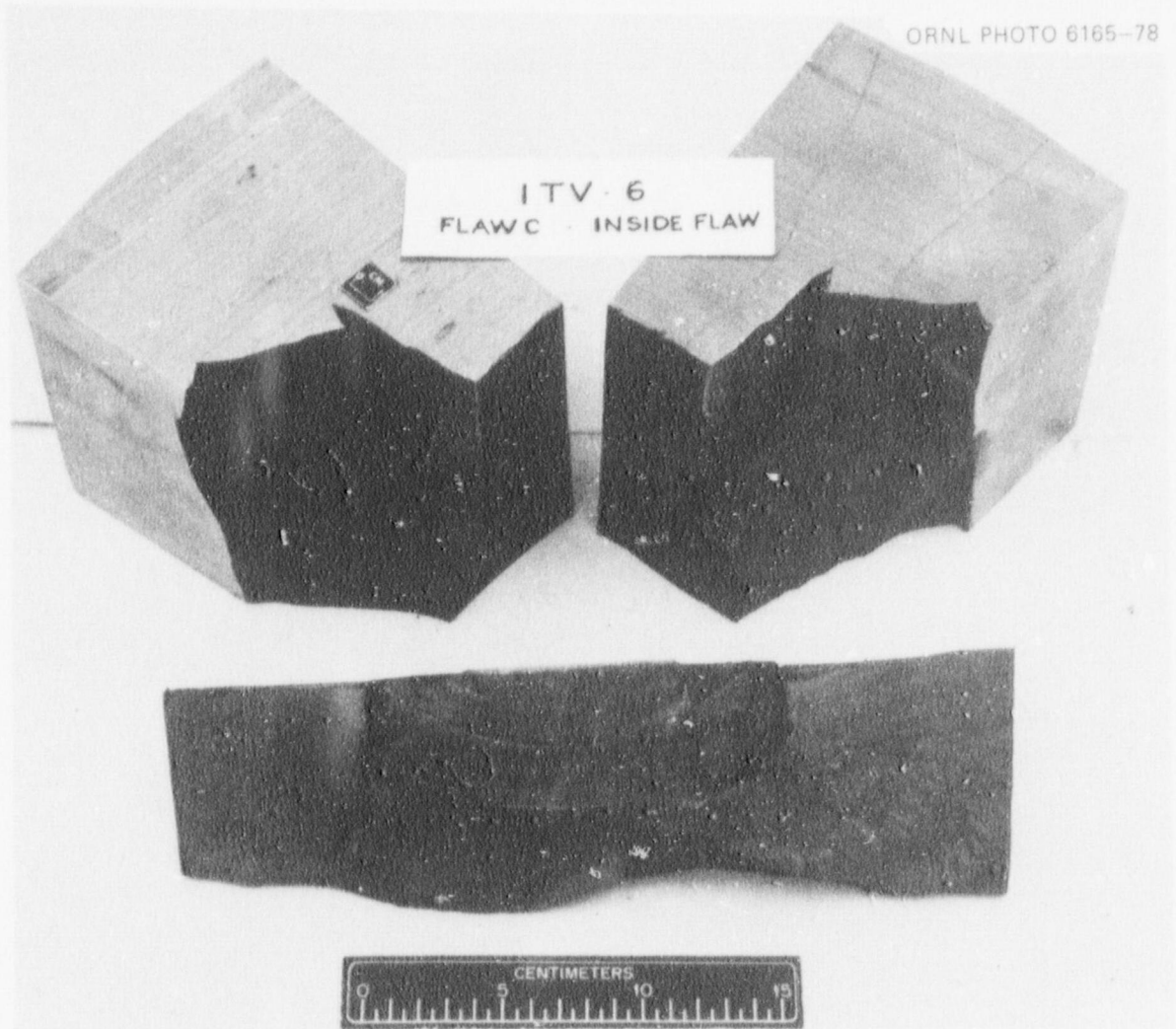


Fig. 5.10. Fracture surfaces and flaw profile of flaw C from intermediate test vessel V-6.

5.5 Crack-Arrest Tests

G. C. Smith

During the reporting period, preparations were made for the ORNL participation in the NRC/EPRI crack-arrest cooperative test effort. Methods of installing ladder-type gages on side grooved specimens were tried, and a satisfactory technique was achieved. Two crack-arrest specimens of the MRL type were machined from A533 material and tested at ORNL. At room temperature, K_{Ia} values of 93 and 90 $\text{MN}\cdot\text{m}^{-3/2}$ were determined. These values fell very near the center of the scatter band reported by Crosley

6. THERMAL SHOCK INVESTIGATIONS*

R. D. Cheverton S. E. Bolt
S. K. Iskander

6.1 Introduction

During this reporting period for the Thermal Shock Program, spray procedures for coating the inner surface of TSV-F in the new vertical spray facility were developed; TSV-F was subjected to two liquid nitrogen (LN_2) thermal shocks in the LN_2 test facility to obtain thermal-hydraulic data; the test facility was redesigned and construction of new components completed; a fracture-mechanics parametric analysis of the PWR double-ended-pipe-break LOCA-ECC was completed; a first draft of the LOCA-ECC thermal shock "significance" report was completed; and preliminary fracture-mechanics calculations pertaining to the PWR steam-like-break accident were performed.

6.2 Cryogenic Quenching

ORNL is attempting to develop a capability for imposing thermal shocks on steel cylinders using LN_2 as the heat sink. The LN_2 quench has certain advantages over other thermal shock techniques considered, not the least of which is lower cost, and is appropriate for proposed future thermal shock experiments.¹

A complication associated with cryogenic quenching is the formation of a nitrogen vapor blanket (film-boiling regime) that drastically retards heat transfer until the film superheat (surface temperature - LN_2 temperature) drops to a few degrees. At this point the nucleate boiling regime is established, and a rapid quench is achieved -- but too late. This difficulty is circumvented by applying a thin layer of insulating material to the metal surface. The insulating effect limits the heat flux initially, allowing the nucleate boiling regime to be established immediately.

* Conversions from SI to English units for all SI quantities are listed on a foldout page at the end of this report.

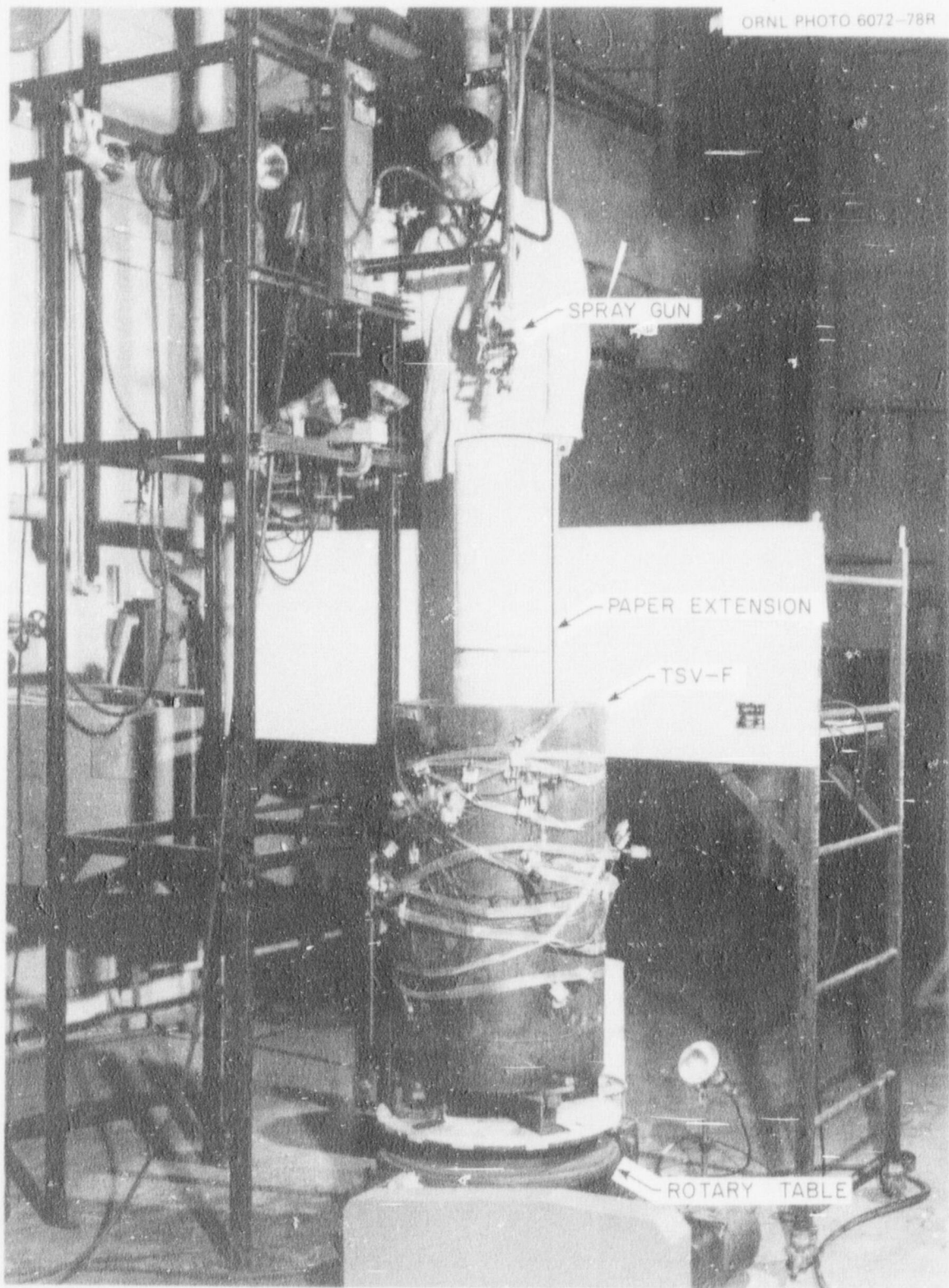
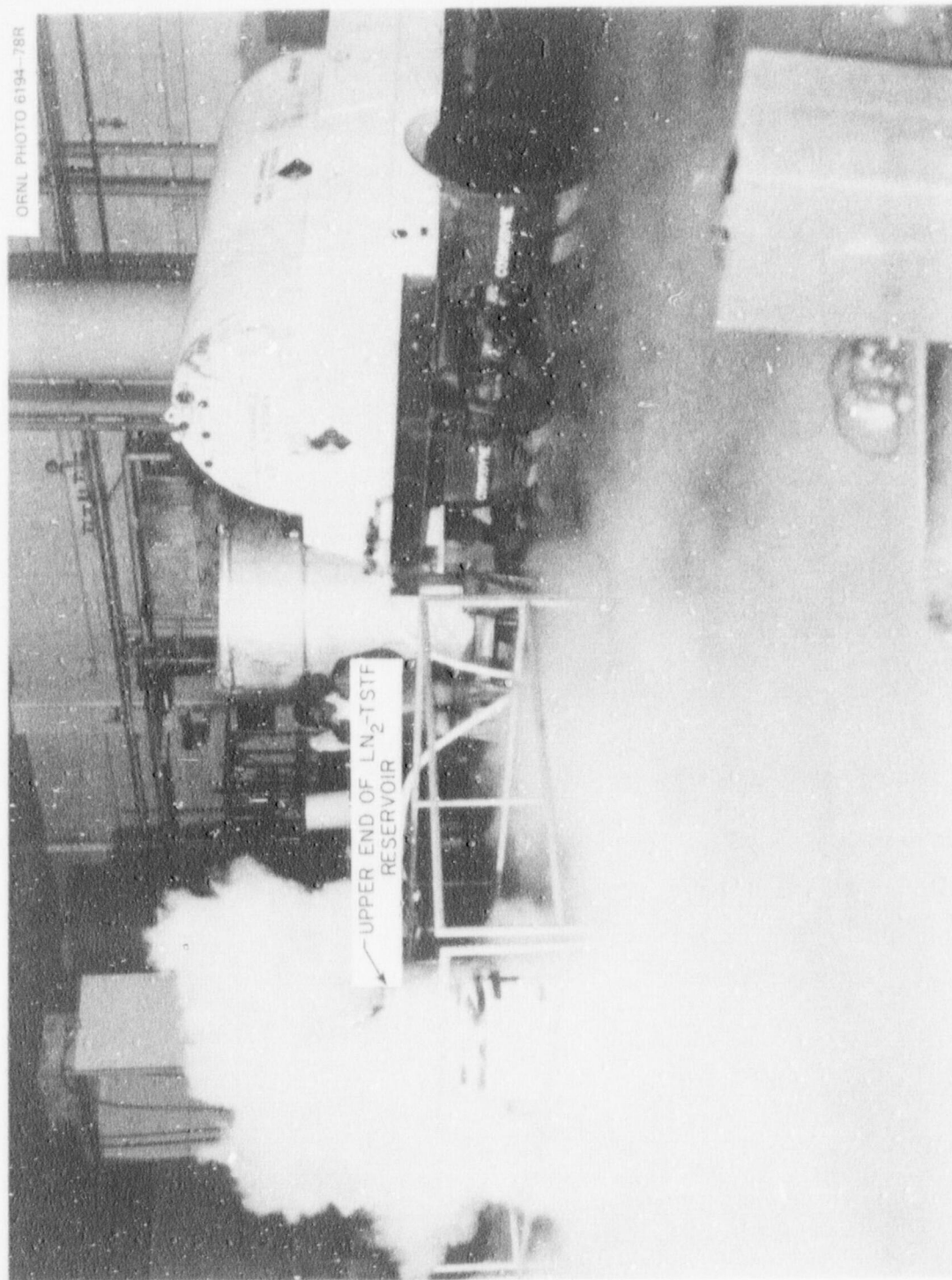


Fig. 6.1. Vertical spray facility.



ORNL PHOTO 5194-78R

Fig. 6.2. Photograph of LN₂-TSTF taken during LN₂-TSE-F(2).

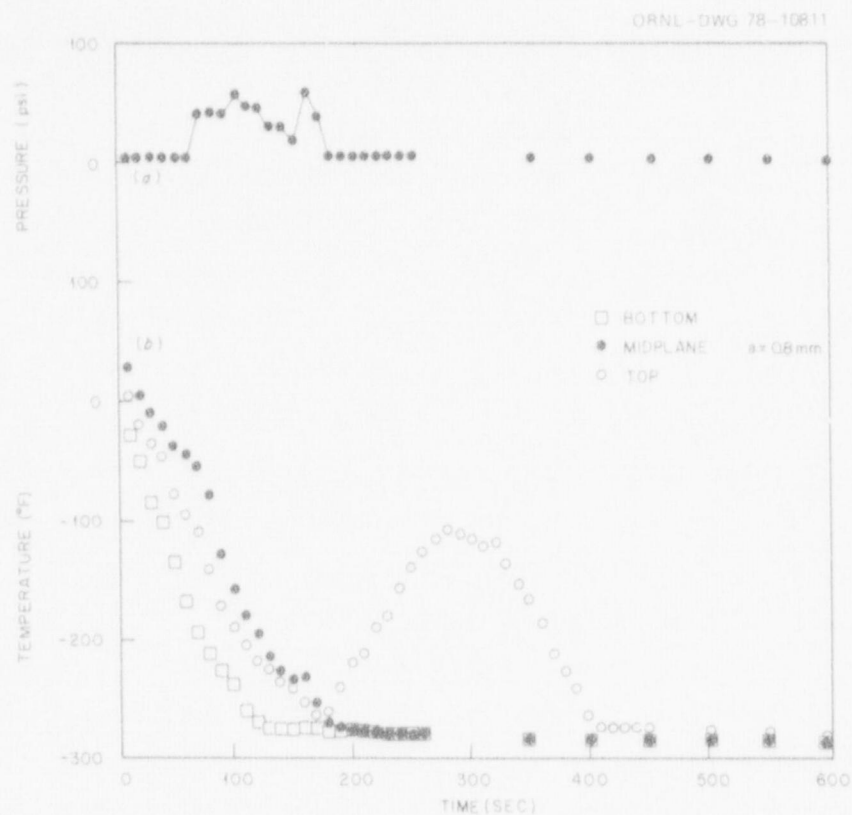


Fig. 6.3. Pump discharge pressure (a); temperature vs time for points ~ 0.8 mm from inner surface during quench of TSV-F with LN_2 initial temperature = 21°C (b). Test $\text{LN}_2\text{-TSE-F}(2)$.

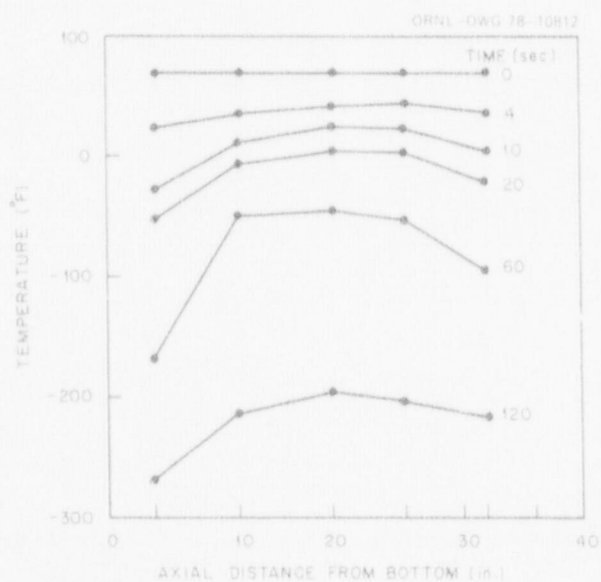


Fig. 6.4. Axial temperature profiles during $\text{LN}_2\text{-TSE-F}(2)$ for points ~ 0.8 mm from inner surface.

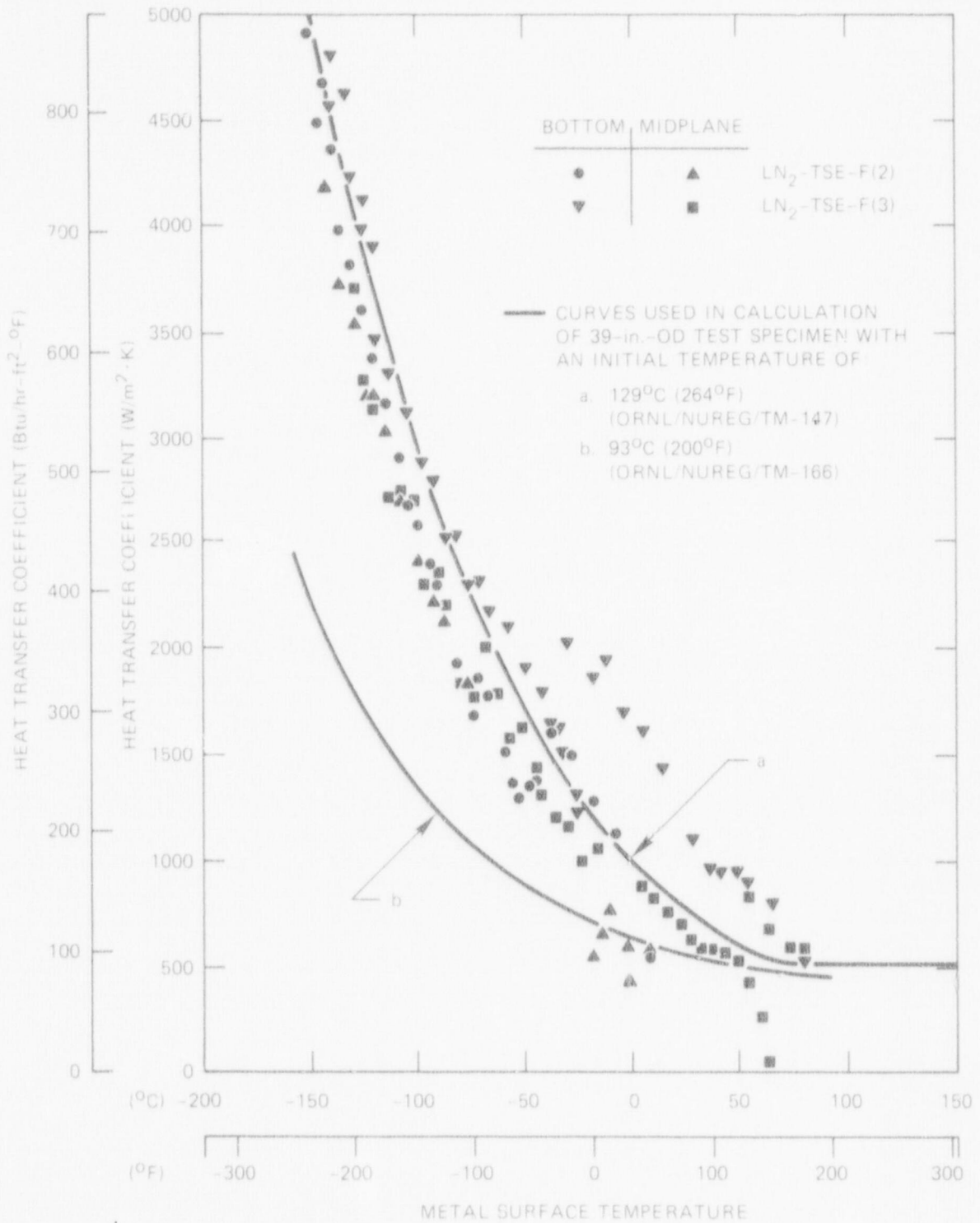


Fig. 6.5. Heat transfer coefficient vs metal surface temperature for LN₂ quench of TSV-F from 21°C and 93°C.

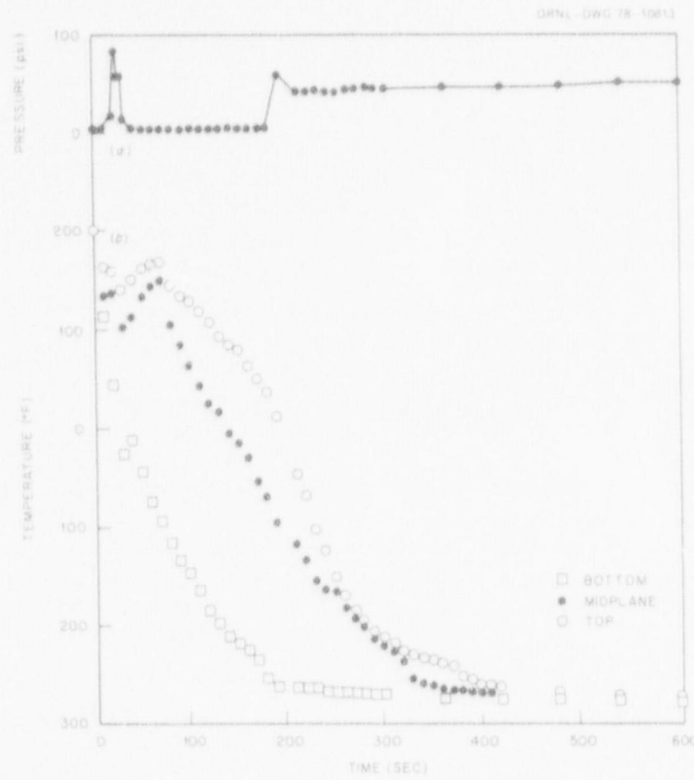


Fig. 6.6. Pump discharge pressure (a); temperature vs time for points ~ 0.8 mm from inner surface during quench of TSV-F with LN_2 initial temperature = 93°C (b). Test LN_2 -TSE-F(3).

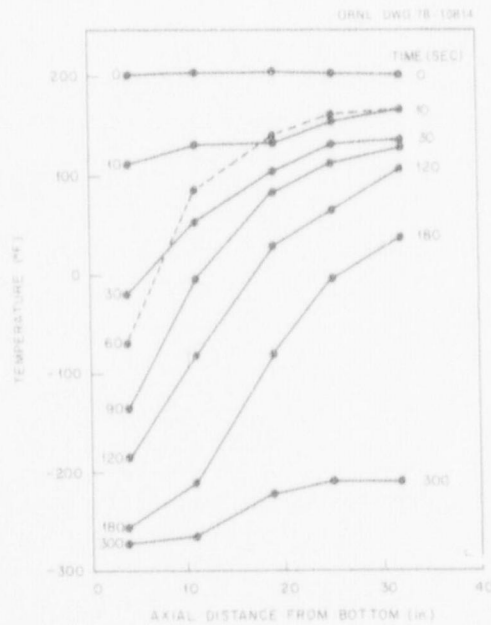


Fig. 6.7. Axial temperature profiles during LN_2 -TSE-F(3) for points ~ 0.8 mm from inner surface.

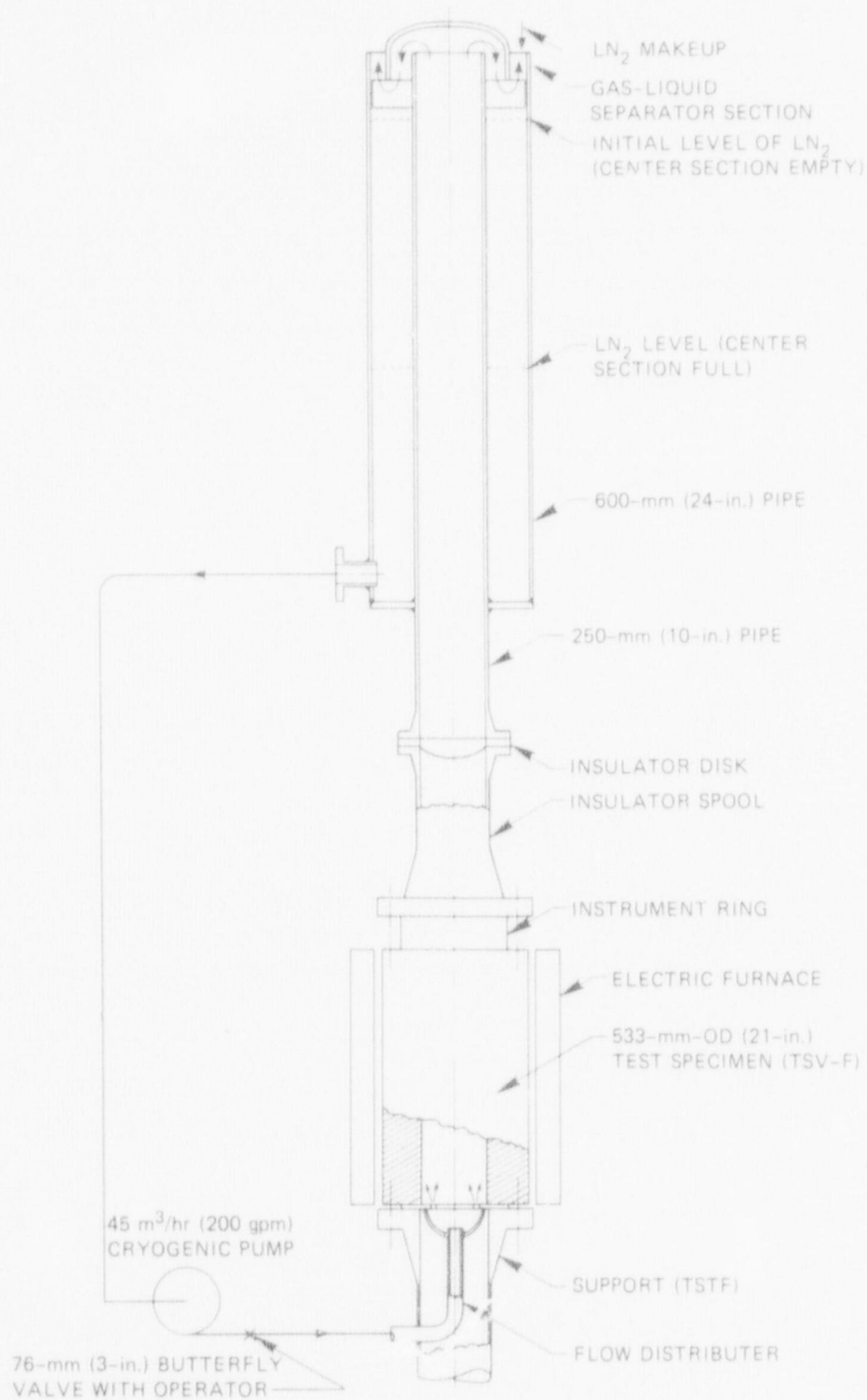


Fig. 6.8. Liquid nitrogen thermal shock test facility [modified design for LN₂-TSE-F(4)].

Table 6.2. Summary of selected results of the RCM double-ended-pipe-break
LOCA-FCC parametric analysis

Flaw	Sink temp. (°F)	Surface fluence (neutrons/cm ²)	RT NDT (°F)	Copper concentration	WPS ^a threshold (a/w)	Maximum arrest depth		Maximum initiation depth without WPS (a/w)
						With WPS (a/w)	Without WPS (a/w)	
Axial	70	4×10^{19}	0	Low	0.25	0.34	>0.8	NI ^b
			0	High				>0.6
			40	Low				NI
			40	High	0.30	0.40	>0.8	>0.6
			80	Low	<0.04	NI-WPS ^c	0.47	0.18
			80	High	0.37	0.50	>0.8	>0.6
			0	Low				NI
			0	High	0.25	0.34	0.60	0.48
			40	Low				NI
			40	High	0.30	0.40	0.70	0.57
			80	Low	<0.03	NI-WPS	0.36	0.17
			80	High	0.37	0.46	3.79	0.67
			40	Low				NI
				High	0.17	0.26	>0.8	>0.6
				Low				NI
				High	0.30	0.40	>0.8	>0.6
				Low	<0.05	NI-WPS	0.35	0.12
				High	0.40	0.52	>0.8	>0.6
			40	Low				NI
				High	0.30	0.40	>0.8	>0.6
				Low				NI
				High	0.30	0.40	>0.8	>0.6
				Low				NI
				High	0.25	0.35	>0.8	0.60

^a Warm prestressed.

^b No initiation since $(K_I/K_{Ic})_{\max} < 1$ for all a/w.

^c No initiation since all cracks with $K_I/K_{Ic} = 1$ are warm prestressed.

Table 7.2 (continued)

Project	Scope	Facility	Remarks
ROSA (contd.)		<p>ROSA-II (For PWR) (1973-1976) This is a modified ROSA-I facility for out-of-pile experiments. The electrical power is 224 kW; there are two coolant loops, designed to study the thermohydraulics of emergency-core cooling with system effects. Each loop has a steam generator and a coolant circulation pump. One loop has valves and equipment for simulating single-ended and double-ended breaks. Simulated vessel internals are used; these include the core, core barrel, flow mixer plate, and core plates.</p> <p>ROSA-III (For BWR) (1977-1979) The ROSA facility will be modified to include a spray system for emergency core cooling.</p>	

